A remote sensing monitoring method for alpine grasslands desertification in the eastern Qinghai–Tibetan Plateau

KUANG Qian[1,2] https://orcid.org/0000-0001-5014-8052; e-mail: 20171103004@stu.sicnu.edu.cn

YUAN Quan-zhi[1,2*] https://orcid.org/0000-0003-0620-8200; ✉e-mail: yuanqz@sicnu.edu.cn

HAN Ji-chong[3] https://orcid.org/0000-0001-9460-0733; e-mail: 201921051199@mail.bnu.edu.cn

LENG Rong[1,2] https://orcid.org/0000-0002-6763-5786; e-mail: 20181101005@stu.sicnu.edu.cn

WANG Yu-shuang[1,2] https://orcid.org//0000-0002-5320-7887; e-mail: 20181101002@stu.sicnu.edu.cn

ZHU Ke-hong[4] https://orcid.org/0000-0001-7353-7595; e-mail: zhukehong@nuctech.com

LIN Shuo[5] https://orcid.org/0000-0002-6775-4363; e-mail: 1144250967@qq.com

REN Ping[1,2] https://orcid.org/0000-0002-3553-0111; e-mail: pren121680@126.com

Corresponding author

1 Key Laboratory of Land Resources Evaluation and Monitoring in Southwest, Ministry of Education, Sichuan Normal University, Chengdu 610068, China

2 Institute of Geography and Resources Science, Sichuan Normal University, Chengdu 610068, China

3 Key Laboratory of Environmental Change and Natural Disaster, MOE/State Key Laboratory of Earth Surface Processes and Resources Ecology, Faculty of Geographical Science, Academy of Disaster Reduction and Emergency Management, Beijing Normal University, Beijing 100875, China

4 Department of Engineering Physics, Tsinghua University, Beijing 100084, China

5 College of Resources, Sichuan Agricultural University, Chengdu 611130, China

Abstract: Alpine grassland is the typical vegetation in the eastern Qinghai–Tibetan Plateau, which has important ecological service functions, and also supports the development of alpine stock farming. In recent years, under both the natural and human disturbance, alpine grasslands in this area have appeared to different degrees of desertification. A diagnosis of the desertification degree serves as the basis for grassland ecological restoration. This study constructs a comprehensive index based on remote sensing called alpine grassland desertification index (AGDI) to monitor the areas and degree of desertification. The most relevant indicators of desertification, namely, vegetation fraction, aboveground biomass, soil moisture, and land surface temperature, were selected to establish AGDI. The geographical detector is used to reselect and assess these indicators. The results show that the overall verification accuracy of AGDI is 82.05%. In particular, the accuracy of identifying severe desertification is the highest. Our study confirms that the desertification of alpine grasslands in the eastern Qinghai–Tibetan Plateau is characterized by fragmentation. Thus, Landsat-8 OLI data with a spatial resolution of 30 m is more suitable than MODIS data for alpine grasslands desertification monitoring. The research results can provide a methodological reference for

monitoring desertification of alpine grasslands and other grassland regions in the world.

Introduction

China has nearly 400 million ha of natural grasslands which occupy 41.7% of its territory and account for approximately 13% of the world's grassland area. However, 90% of China's available natural grasslands exhibit varying degrees of degradation, half of which are manifested in terms of reduced vegetative coverage, desertification, salinization, and other characteristics of moderate or severe degradation (Development Planning Department of Agriculture 2003). Grassland desertification is one of the most important aspects in the degradation context (Reynolds et al. 2007; Bestelmeyer et al. 2015; Qin et al. 2016). Grassland desertification indicates that natural grasslands have suffered from various degrees of damage, such as wind erosion, drought, and overgrazing, thereby turning the grasslands into a desert-like landscape (Li et al. 2013). At present, 20% of the world's land area are threatened by desertification (Wang et al. 2016). Grassland desertification severely affects the balance of global grassland ecosystems, thereby resulting in water erosion, drought, and soil fertility decline. Accordingly, the desertification research field needs accurate monitoring and a diagnosis of the condition of desertification (Rubio and Bochet 1998; Huang and Siegert 2006; Sepehr and Zucca 2012). Over the years, remote sensing data and technology that offer extensive information and precise and rapidly updated data have been used widely in the grassland desertification research (Wang et al. 2010; Mansour et al. 2016; Wen et al. 2010; Zhang et al. 2019).

Previous studies have used visual interpretation combined with image processing software to classify the types and levels of desertification (Kuang et al. 2002; Wang et al. 2008; Li et al. 2013; Del Valle et al. 2014). Kuang et al. (2002) focused on land desertification investigation of the agriculture and graziery mixed area in the Duolun region of Inner Mongolia, and

mainly used artificial interpretation by TM (Thematic Mapper) image. Li et al. (2013) used the 1990, 2000, and 2010 Landsat images of Northern Tibet as bases to classify the main grassland landscape by hybrid classification method and analyze the characteristics of the landscape patterns and grassland degradation through landscape index. Visual interpretation and field surveys are the reliable method to obtain the result of grassland desertification. However, this method is time-consuming and laborious when monitoring large areas.

The majority of related studies have focused on vegetation characteristics, such as, vegetation coverage (Gao et al. 2010; Rossi et al. 2019; Zhang et al. 2014), grassland productivity (Tsunekawa et al. 2005; Brinkmann et al. 2011), and aboveground biomass (Li et al. 2006), to evaluate desertification. With the development of remote sensing index, some studies have chosen vegetation indices related to desertification, such as normalized difference vegetation index (NDVI), enhanced vegetation index (EVI), ratio vegetation index (RVI), and net primary productivity (NPP), to evaluate the situation and dynamic changes of grassland desertification (Gao et al. 2010; Zhou et al. 2017). Gao et al. (2010) used MODIS-NDVI data to assess alpine grassland degradation between 1981 and 2004 in Northern Tibet, and examined trends in grassland degradation and its response to climate variability. Zhou et al. (2017) selected net primary productivity (NPP) and grass coverage as indicators to analyze grassland degradation dynamics. And they designed a method to assess the driving force of grassland degradation based on NPP. These methods are easy to quantify and substantially maximize the advantages of remote sensing data. However, measuring grassland desertification solely by vegetation index has certain limitations because grassland desertification is the comprehensive result of the interactions of soil, vegetation, and other factors (Schlesinger et al. 1990). Thus, considering multiple characteristics to evaluate grassland desertification is a considerably scientific approach. Becerril et al. (2016) constructed an integrated desertification degree index (DDI) based on the NDVI–Albedo relationship, and evaluated the desertification of a semi-arid zone in Querétaro state. Lamqadem et al. (2018) developed DDI using the tasselled cap wetness (TCW) and tasselled cap

1424

brightness (TCB) features, and used DDI to map the desertification degree of the central-southern region of Morocco. Although these studies have combined the remote sensing index of vegetation and soil, their ecological significance is unclear. That is, they have failed to prove that these indices, TCB and TCW, are directly related to grassland desertification. Evidently, constructing an index with clear ecological meaning is easy to understand and promote in other areas.

The eastern margin of the Qinghai–Tibetan Plateau is a water conservation area and ecological barrier for some important hydrographic systems (e.g., Yangtze River, Yellow River, and Lancang River), characterized by a humid or semi-humid climate (Yuan et al. 2017; Zhang et al. 2019). Alpine grasslands are typical vegetation type on the plateau that have high yield and good quality and an important development area for alpine stock farming (Yu et al. 2016; Yue et al. 2018). The alpine grasslands on the Qinghai–Tibetan Plateau

comprise 38% of the total grassland area in China (Zhao et al. 2012). In recent decades, the desertification of alpine grasslands has become serious, with a trend of reverse succession. Grassland coverage is decreasing, while the ecosystem fragility is increasing, thereby affecting the sustainable development of the stock economy and threatening the ecological security of the Yangtze and Yellow River source regions (Dong et al. 2010; Li et al. 2013).

Given the preceding situation, this paper proposes an aggregative index called alpine grassland desertification index (AGDI) to quantify the degree of desertification in alpine grasslands. Four ecological indicators and geographical detector (See Section 2.3.1: Geographical detector) were used to construct AGDI. The current study aims to provide a methodological reference for monitoring alpine grassland desertification and identifying areas at risk of desertification. Accurate monitoring of alpine grassland desertification in Qinghai–Tibetan Plateau is important for grassland management and sustainable development of the stock economy.

1 Materials

1.1 Study area

Zoige County is located on the eastern Qinghai-Tibetan Plateau, at the junction of China's Sichuan, Gansu, and Qinghai provinces, between 32°56'- 34°19' N, 102°08' -103°39' E (Figure 1). Zoige has a total area of 10436 km² with an average elevation of 3500 m above sea level, wherein 76.12% of the area is covered by alpine grasslands (He et al. 2016). The climate of the Zoige grasslands is typical of alpine regions. The annual
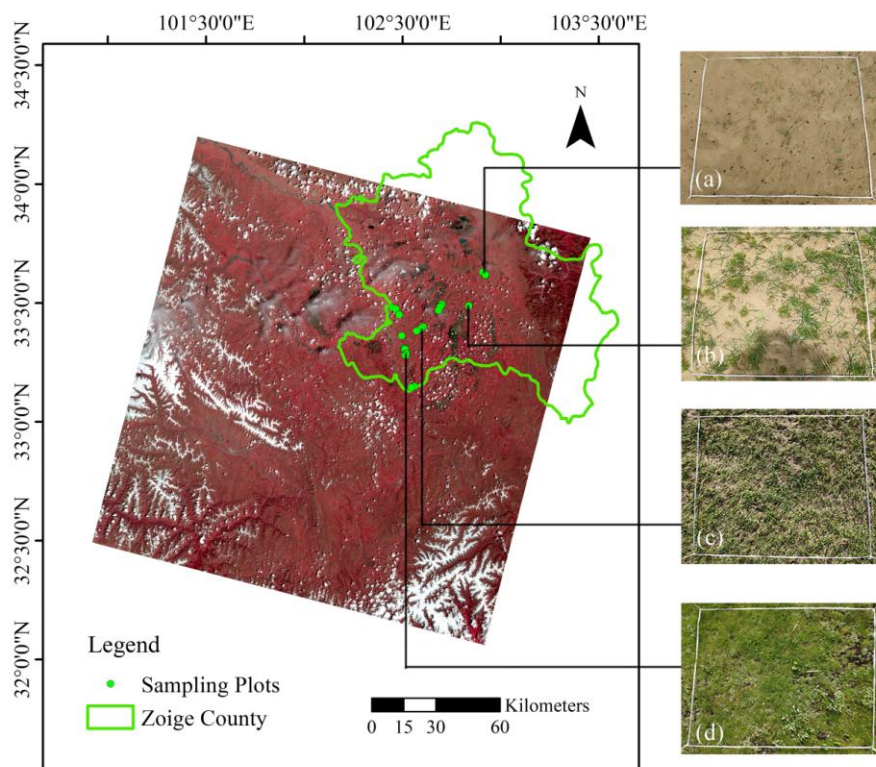
Figure 1 Geographical location of the study area and field sampling plots distribution. The Landsat 8 OLI (Operational Land Imager) image of the study area was obtained in May 2019 and was the RGB (red, green, blue) composite of Landsat bands 5, 4, and 3. The images on the right are the sampling photos of the varying degrees of desertification: (a) severe desertification (SD), (b) moderate desertification (MD), (c) light desertification (LD), and (d) non-desertification (ND).

1425

mean temperature is 1.4°C and the average annual mean precipitation is 642.8 mm (mainly concentrated in June–August) (Shui et al. 2017). Zoige is dominated by alpine livestock farming as alpine grasslands provide forage for cattle or yaks by grazing or producing hay or silage. Zoige's plant growing period is from late March to early September.

Zoige is an important part of the source area of the Yellow River. This county has an impact on the ecological environment construction and protection of the source area of the Yellow River, as well as the sustainable development of the entire Yellow River basin (Qiu 2016). However, Zoige experienced such problems as wetland shrinkage and grassland degradation because of the dual influence of natural environment change and unreasonable human activities (Hu et al. 2013). In the Zoige Basin, the degraded grasslands increased by 627 km² from 1994 to 2009 (Yu et al. 2017). Accordingly, considerable attention has been provided to the desertification problem in the Zoige grasslands (Wang et al. 2015; Gou et al. 2016; Wang et al. 2016). We specifically choose Zoige as our study area owing to its special geographical location and economic advantages.

1.2 Remote sensing data and preprocessing

Landsat-8 OLI data (the main remote sensing data) were used in this study, with a spatial resolution of 30 m. Zoige is covered by four images, namely, path 131-row 37, path 131-row 36, path 130-row 37, and path 130-row 36. We selected path 131-row 37 for May 21, 2019, which was near the sampling time, owing to cloud coverage, image strip noise, measured data time, and other consideration of data quality. This image covered over 89% of the grassland area in Zoige, thereby meeting our research needs.

Firstly, the Landsat-8 OLI data were subjected to a series of preprocessing, such as radiometric calibration, atmospheric correction, and cropping. To reduce the impact of clouds and the shadow they cast on the ground, a mask was created for the area covered by clouds in Zoige. Secondly, we obtained the Zoige grassland coverage map using the object-oriented automatic classification method. The use of field verification points verified this map, and the classification accuracy of grasslands

reached 91%. Thirdly, three common vegetation indices were calculated: NDVI, EVI, and RVI. In addition, three characteristic variables, i.e., TCB, TCW, and tasselled cap greenness (TCG), were obtained using Tasseled cap transformation (Kauth and Thomas 1976). TCB reveals the bright soil with bare land and the absence of vegetation. TCW corresponds to soil moisture. Lastly, TCG represents the different types and densities of vegetation coverage (Zanchetta et al. 2016).

We selected the MOD11A2 product (Land Surface Temperature/Emissivity 8-Day L3 Global 1 km) to retrieve the land surface temperature (Hengl et al. 2012). We chose eight images in May–June 2019 (i.e., May 1, May 9, May 17, May 25, June 2, June 10, June 18, and June 26), when the grasslands returned to green. Zoige is covered by tile h26v05. For the preprocessing of MOD11A2, the format conversion and re-projection were performed using the MODIS Conversion Toolkit. The projection coordinate system is defined as the Albers projection system. The maximum value composite method was used to remove outliers for the effects of clouds, atmosphere, and solar elevation angle. Moreover, we resampled the result using cubic convolution at 30 m to address the difference in spatial resolution. Then we calculated vegetation supply water index (VSWI) (Chu 2018) and temperature vegetation dryness index (TVDI) (Wang et al. 2016; Cao et al. 2017) for retrieving soil moisture.

1.3 Field survey data and preprocessing

A total of 39 sampling plots (30 m × 30 m) of varying degrees of desertification were surveyed in Zoige (Figure 1), in June 2019. Each of the plots was sampled with one 1 m × 1 m quadrat in the center. Soil moisture, land surface temperature, aboveground biomass and vegetation characteristics were measured in small quadrats. We used the soil analyzer TZS-ECW to measure the land surface temperature and soil moisture in quadrats. Moreover, we referred to China's national natural grassland degradation, desertification, and salinization classification index standards to define the degree of desertification of plots as severe desertification (SD), moderate desertification (MD), light desertification (LD), and non-desertification (ND) (Ministry of agriculture

2003). Thereafter, 3–5 quadrats' photos were taken vertically to calculate the vegetation coverage. Lastly, the aboveground plants in the quadrat was clipped, dried, and weighed to obtain the field aboveground biomass data.

2 Methods

2.1 Basic theory for constructing Alpine Grassland Desertification Index (AGDI)

Loss of vegetation coverage and soil erosion are the most visible signs of desertification (Galindo et al. 2008). Therefore, AGDI integrates vegetation and soil characteristics of grassland desertification and is calculated using remote sensing index which is most relevant to the ecological significance of grassland desertification. Firstly based on the principles of scientificity, representativeness, and accessibility, we initially select four ecological indicators, namely, vegetation fraction (VF), aboveground biomass (AGB), soil moisture (SM), and land surface temperature (LST), which are most relevant to the symptoms of desertification. In the vegetation layer, VF is the most common indicator used to classify the degree of desertification. The worse the degree of desertification, the lower the vegetation coverage (Rossi et al. 2019). Grassland desertification changes the stability of the plant community. Consequently, AGB is reduced (Han et al. 2018). AGB is closely related to soil nutrient and grassland productivity, and can express plant height and aboveground productivity that cannot be shown by vegetation coverage (Jin et al. 2014; Zhang et al. 2016). In the soil layer, SM is the main ecological limiting factor of grassland desertification (Chang et al. 2017). Grassland desertification is accompanied by soil erosion, which leads to soil moisture decrease. Soil moisture is higher in non-desertification

areas than desertification area (Zhang et al. 2016). Although rainfall permeates into the soil and increases soil moisture, the period before wet season was chosen to reduce the effects of atmospheric precipitation (He et al. 2015). LST shows the difference of underlying surface. Even at the same temperature, the land surface temperatures of bare soil and grasslands are different from each other (Chang et al. 2012). Second, ecological indicators were estimated. VF was calculated from NDVI using the dimidiate pixel model, and LST was derived from MOD11A2 (Li 2003). To obtain AGB and SM, the remote sensing index relating the two indicators were combined with measured date to establish univariate regression models. The most suitable formula with remote sensing index is used to calculate the two indicators. Third, the estimation results and in situ measured data indicate that all indicators were discretized to four grades corresponding to the desertification degree. These indicators were selected again and weighed using a geographical detector to construct AGDI. Figure 2
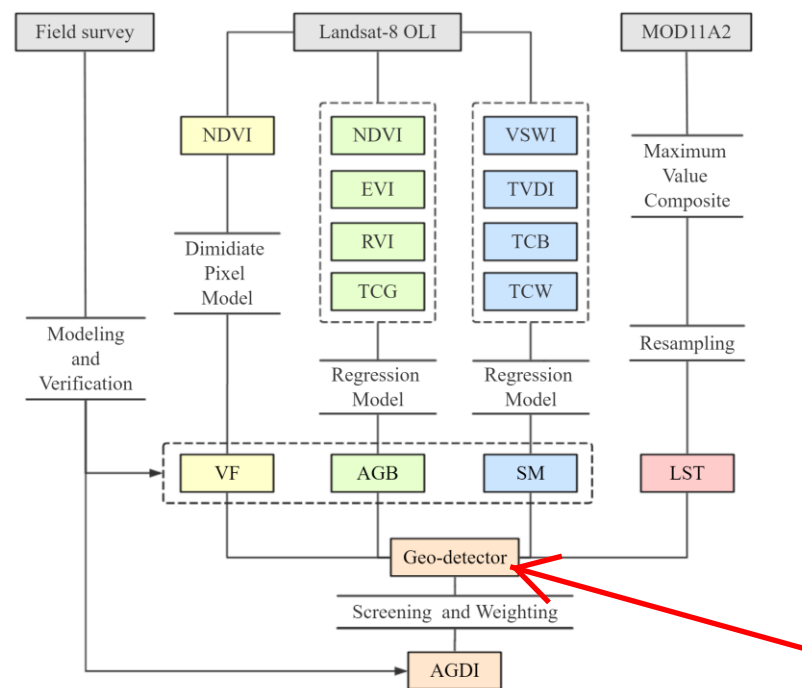
Figure 2 Flowchart of establishing alpine grassland desertification index (AGDI). NDVI: normalized difference vegetation index, VSWI: vegetation supply water index, EVI: enhanced vegetation index, TVDI: temperature vegetation dryness index, RVI: ratio vegetation index, TCB: tasselled cap brightness, TCG: tasselled cap greenness, TCW: tasselled cap wetness, VF: vegetation fraction, AGB: aboveground biomass, SM: soil moisture, LST: land surface temperature, and Geo-detector: geographical detector.

1427

shows the process for calculating AGDI.

2.2 Estimation of the indicators

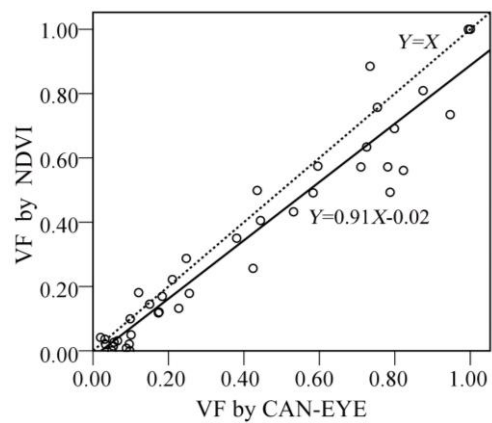### 2.2.1 Vegetation fraction (VF) estimation

We input the photos taken by the quadrats into the software CAN-EYE (version 636), which is developed by the French National Institute of Agricultural Research and uses true color images to extract vegetation characteristics (including vegetation cover fraction, leaf area index, average leaf inclination an-gle, etc.) (Demarez et al. 2008; Mougin et al. 2014). CAN-EYE extracted vegetation information using the RGB (red, green, blue) values on the sampling photos, and set specific threshold to obtain the vegetation fraction from the field survey. Thereafter, the dimidiate pixel model was introduced to calculate the simulated vegetation fraction:

$$VF = \frac{NDVI - NDVI_{soil}}{NDVI_{veg} - NDVI_{soil}} \quad (1)$$

where $NDVI_{soil}$ is the NDVI value of the bare or non-vegetation covered area and $NDVI_{veg}$ is the NDVI value of the pixel completely covered by vegetation (i.e., NDVI value of the pure vegetation pixel). The key aspect of the model is how to accurately obtain the value of $NDVI_{soil}$ and $NDVI_{veg}$ (Li 2003). The measured VF of the existing samples indicate that when VF = 0, NDVI = 0.1, i.e., $NDVI_{soil}$ = 0.1; and when VF = 1, NDVI = 0.7, i.e., $NDVI_{veg}$ = 0.7. Therefore, the simulated VF result was obtained and compared with the measured VF, as shown in Figure 3. The $Y = X$ equation regression line, Pearson correlation coefficient (r), and root mean squared error ($RMSE$) were used to verify the accuracy between the simulated and measured values.

$$RMSE = \sqrt{\frac{1}{n}\sum_{i=1}^{n}(y_i - y_i')^2} \quad (2)$$

where y_i and y_i' are the measured and simulated values, respectively, and n is the number of samples. Figure 3 shows the comparison between the field-measured values and simulated values. Comparing to the middle and low vegetation coverage samples, the high vegetation coverage samples deviated substantially from $Y = X$. Thereby indicating that the accuracy of the high vegetation

Figure 3 Linear regression of the field-measured values (x-axis) and simulated values (y-axis) for vegetation fraction (VF) (n = 39). Simulated values were calculated from Equation (1), and field-measured values were calculated by software CAN-EYE (version 636).

coverage samples is lower than the other degree of vegetation coverage. All scatter plots were approximately distributed around $Y = X$. Furthermore, r = 0.97 between the measured and simulated values was highly correlated. $RMSE$ = 0.10. The smaller the $RMSE$, the lower the difference between the true and the measured values. Thus, the research accuracy is satisfied.

2.2.2 Aboveground biomass (AGB) estimation

A total of 28 sampling points distributed equally in areas with the different desertification degree were selected randomly. To select a suitable index used to retrieve AGB, univariate regression models combined measured AGB with vegetation indices (NDVI, EVI, RVI) and TCG were established. Firstly, selecting the model entails focusing on whether the model passes the significance test. Secondly, the actual change of AGB in alpine grasslands and the coefficient of determination (R^2) should be considered. Thirdly, the accuracy of the model should be verified. TCG was excluded because the models established by TCG and AGB did not pass the significance test. Table 1 shows the regression models that passed the significance test. The cubic regression equation was set aside because of its inconsistencies and extreme values, which do not meet the actual changes of AGB. At this time, the R^2 of the logarithm and reciprocal regression model established by AGB−EVI was higher than the R^2 of the model established by other indices. Therefore,

Table 1 Regression models of Aboveground Biomass (AGB). Selected indices and models in estimating AGB. *F*: F-test Value; Sig.: Statistical significance.

Models	AGB−EVI			AGB−NDVI			AGB−RVI		
	R^2	F	Sig.	R^2	F	Sig.	R^2	F	Sig.
Logarithmic model	0.406	25.32	0.000	0.375	22.23	0.000	/	/	/
Reciprocal model	0.380	22.71	0.000	0.361	20.97	0.000	0.368	21.51	0.000
Cubic model	0.485	11.00	0.000	/	/	/	0.510	12.14	0.000

Notes: EVI = enhanced vegetation index; NDVI =normalized difference vegetation index; RVI =ratio vegetation index

Table 2 Regression models of Soil Moisture (SM). Selected indices and models in estimating SM. *F*: F-test Value; Sig.: Statistical significance.

Models	SM−VSWI			SM−TCB			SM−TCW		
	R^2	F	Sig.	R^2	F	Sig.	R^2	F	Sig.
Linear model	/	/	/	0.203	9.40	0.004	0.270	13.72	0.001
Logarithmic model	0.522	40.34	0.000	0.375	22.23	0.000	/	/	/
Reciprocal model	0.410	25.07	0.000	/	/	/	0.389	23.55	0.000
Exponential mode	0.665	73.61	0.000	/	/	/	0.267	13.51	0.001
Quadratic model	/	/	/	0.230	11.08	0.002	0.358	10.03	0.000

Note: VSWI =vegetation supply water index; TCB= tasselled cap brightness; TCW =tasselled cap wetness.
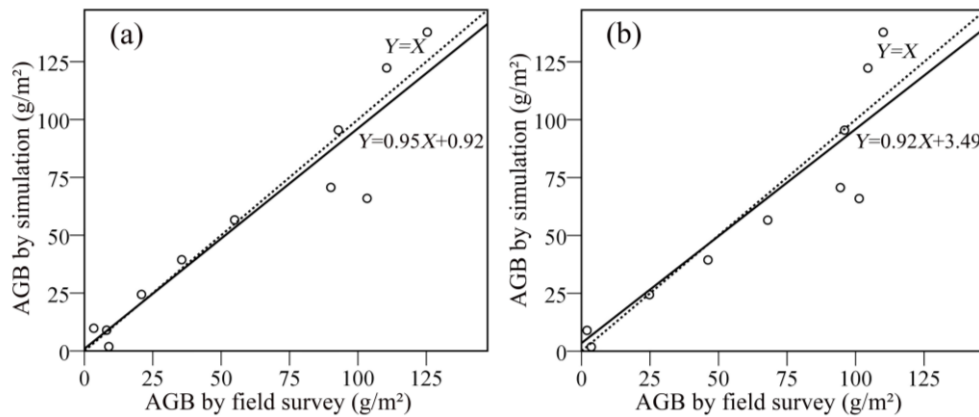
Figure 4 Linear regression of the field-measured values (*x*-axis) and simulated values (*y*-axis) for aboveground biomass (AGB) (*n* = 11). Simulated values were calculated based on the models of AGB−EVI (aboveground biomass - enhanced vegetation index) in Table 2: (a) logarithmic model and (b) reciprocal model.

the accuracy of the AGB−EVI logarithmic model and the reciprocal model were verified by the rest of the sampling points, as shown in Figure 4.

Figure 4 shows that the measured and simulated values of the two models were around the *Y* = *X* line, except two points. From the Pearson correlation coefficient, the logarithmic model (*r* = 0.95) was higher than the reciprocal model (*r* = 0.92). A comparison of *RMSE* of two models shows that the logarithmic model (*RMSE* = 14.14 g/m²) was lower than the reciprocal model (*RMSE* = 17.65 g/m²). The simulation result of the logarithmic model was close to the measured value. In summary, the AGB-EVI logarithmic regression model was selected to retrieve AGB. The regression equation is as follows:

$$AGB = 66.428 \ln EVI + 183.140 \quad (3)$$

2.2.3 Soil moisture (SM) estimation

Univariate regression models were established using the measured SM of the 28 samples with TVDI, VSWI, TCB, and TCW. Among these models, the regression models of SM−TVDI did not pass the significance test. Thus, TVDI was excluded. Table 2 shows the remainder of the regression models. In this table, the models' R^2 established by SM−VSWI was higher than other models' R^2. Therefore, the accuracy of the SM−VSWI models were verified, as shown in Figure 5.

Figure 5 shows that the points of the exponential model distributed around the *Y* = *X*

line were closer than those of the other models. However, the distribution of the other models was not good. For the Pearson correlation coefficient, exponential model ($r = 0.8$) > logarithmic model ($r = 0.66$) > reciprocal model ($r = 0.57$). For the comparison of *RMSE*, the exponential model (*RMSE* = 7.4%) < logarithmic model (*RMSE* = 9.09%) < reciprocal model (*RMSE* = 10.03%) were considered. Hence, the SM–VSWI exponential regression model was selected to retrieve soil moisture. The regression equation is as follows:

$$SM = 7.41e^{654.675 \times VSWI} \quad (4)$$

2.3 Construction of Alpine Grassland Desertification Index (AGDI)

2.3.1 Geographical detector

This study used factor detector to select reasonable indicators and determine their weights to construct AGDI. Geographical detector (Geo-detector) is a novel tool used to explore spatial stratified heterogeneity (SSH) and attribute the spatial patterns. This tool has been widely used in the factor detection studies of spatial heterogeneity(Du et al. 2016; Zhang and Zhao 2018; Bai et al. 2019). This tool can investigate the interaction between explanatory variables $X_1, X_2, ..., X_n$ to a response variable Y by the following geographical detector *q*-statistic:

$$q = 1 - \frac{1}{N\sigma^2} \sum_{h=1}^{L} N_h \sigma_h^2 \quad (5)$$

where N and σ^2 are the number of units and variance of *Y*, respectively, in a study area. Population *Y* is composed of *L* strata ($h = 1, 2, ..., L$).

The strata of *Y* are a partition of *Y*, either by itself *h(Y)* or by an explanatory variable *X,* which is a categorical *h(X)*. The value *X* should be stratified. If *X* is a numerical variable, then the number of strata *L* may be 2–10 or more, according to prior knowledge or a classification algorithm (Wang 2017). In the factor detector, the *q*-statistic measures SSH of a variable *Y*, or the determinant power of an explanatory variable *X* of *Y*. The value of *q* is strictly within [0, 1]. Furthermore, *q* = 1 indicates that *Y* is completely determined by *X* (i.e., *X* explains 100% of *Y)*. Thereafter, *q* = 0 indicates no coupling relationship between *Y* and *X* (Wang et al. 2016). Geo-detector is good at analyzing type variables. The explanatory variable *X* has to approximate the categorical variable when *X* is a continuous variable. Geo-detectors can achieve high statistical accuracy with small sample sizes (<30). Moreover, the principle of geo-detector avoids multiple independent variable collinearity(Wang and Xu 2017).

2.3.2 Construction of alpine grassland desertification index (AGDI)

Firstly, the four degree of desertification in the field survey points (i.e., SD, MD, LD, and ND) were assigned the values 1, 2, 3, and 4, respectively. These values were introduced in the geo-detector as the dependent variable *Y*.

Secondly, the simulated values of VF, AGB, SM, and LST were obtained using the preceding calculation. Given that these indicators are continuous values, every indicator was discretized as 4 grades based on the correspondence between indicators and each degree of desertification, as shown in Figure 6. These indicators, except LST,
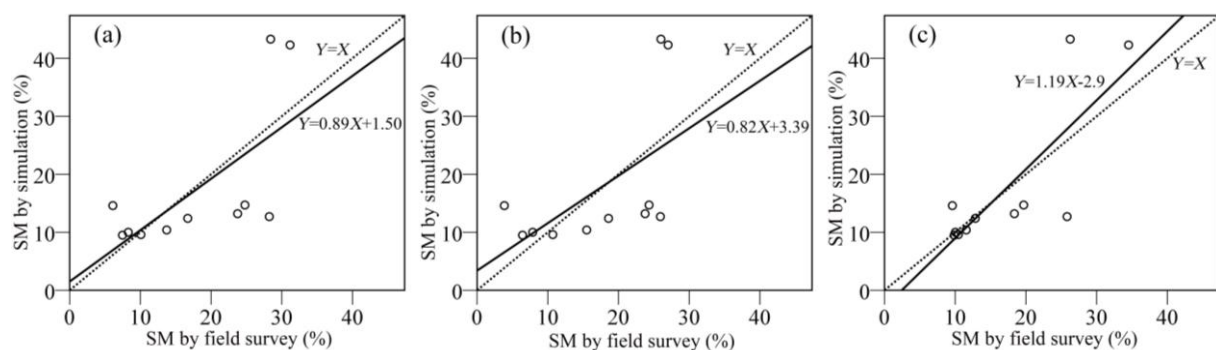
Figure 5 Linear regression of the field-measured values (*x*-axis) and simulated values (*y*-axis) for soil moisture (SM) (*n* = 11). Simulated values were calculated based on the models of SM–VSWI (soil moisture-vegetation supply water index) in Table 3. (a) logarithmic model, (b) reciprocal model, and (c) exponential model.

1430
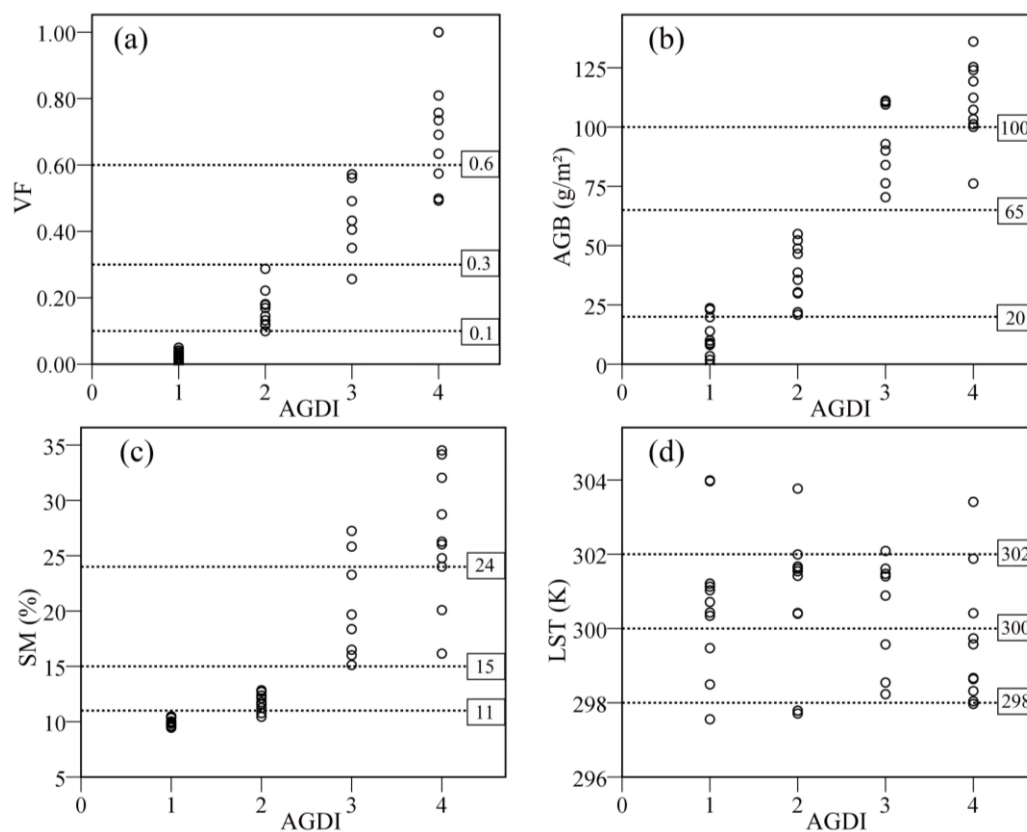
Figure 6 The relationship between alpine grassland desertification index (AGDI) with the indicators: (a) relationship between AGDI and vegetation fraction (VF), (b) relationship between AGDI and aboveground biomass (AGB), (c) relationship between AGDI and soil moisture (SM), and (d) relationship between AGDI and land surface temperature (LST).

Table 3 Indicators' interval related to the desertification degree.

Index	Desertification degree			
	Severe	Moderate	Light	No
AGDI	1	2	3	4
Vegetation fraction (VF)	0〜<0.1	0.1〜<0.30	0.30〜<0.6	0.6〜<1.0
Aboveground biomass (AGB) (g/m²)	0〜<20	20〜<65	65〜<100	>100
Soil moisture (SM) (%)	0〜<11	11〜<15	15〜<24	> 24
Land surface temperature (LST)(K)	> 302.0	300.0〜<302.0	298.0〜<300.0	< 298.0
Assigned value	1	2	3	4

Notes: AGDI =alpine grassland desertification index.

can locate different intervals in the diverse degree of desertification. Table 3 shows the specific intervals of classification. Similarly, each interval of indicator was assigned a value of 1, 2, 3, and 4 as a type variable into the geo-detector. Table 4 shows the result of q-statistic.

Table 4 shows that LST has the weakest interpretation of AGDI among the four primary selected indicators. The value $P > 0.05$ indicates that LST does not pass the significance test. Thus, the indicator was excluded in the construction of AGDI. LST has no apparent correlation with the

Table 4 The result of q-statistic by geographical detector

	VF	AGB	SM	LST
q	0.924	0.908	0.907	0.167
P	0.000	0.000	0.000	0.258

Note: For the meanings of the abbreviations in the table head, please refer to the note of Table 3.

classification of AGDI in Figure 6(d). By contrast, VF, AGB, and SM had strong explanatory power for AGDI. The result of the q-statistic proved that using the three indicators to evaluate alpine grassland desertification has reference value. Lastly,

1431

the "weighted voting" method was used to establish AGDI. The result of the q-statistic was used as weight. AGDI can be obtained using the following formula:

$$AGDI = \frac{0.924 \times VF + 0.908 \times AGB + 0.907 \times SM}{2.739} \quad (6)$$

3   Results

The spatial distribution of AGDI of study area is shown in Figure 7. This spatial distribution performed on the grassland coverage map was classified by Landsat-8 OLI. In the grassland coverage map, we mask clouds and other land cover types (including construction land, farmland, water, swamp, etc.) and exclude pattern spots of under 3 pixels to reduce the influence of noise. Confusion matrix is used to evaluate the accuracy of classification, which is a commonly used method for detecting the difference between classification

result and in situ information(Foody 2002) (Tables 5 and 6).

For one class: A, User's accuracy is the probability that the corresponding surface category is A when the classifier classifies pixels into category A, and is the probability of representation sampling classification points same as the actual situation on the ground. Producer's accuracy is the probability that classifier can classify an image's pixels as A when the surface is class A, thereby indicating the probability that the ground sampling points are correctly classified. The overall accuracy is the probability that the classified results for each sample are consistent with the actual type of the corresponding area on the ground (Stuckens et al. 2000). Comparing the calculated AGDI and in situ AGDI of samples, the overall accuracy is 82.05%. When the desertification degree is SD, AGDI fully recognizes it through the proposed method. The predicted MD are consistent with the in situ values. The accuracy of LD and ND is relatively low, and
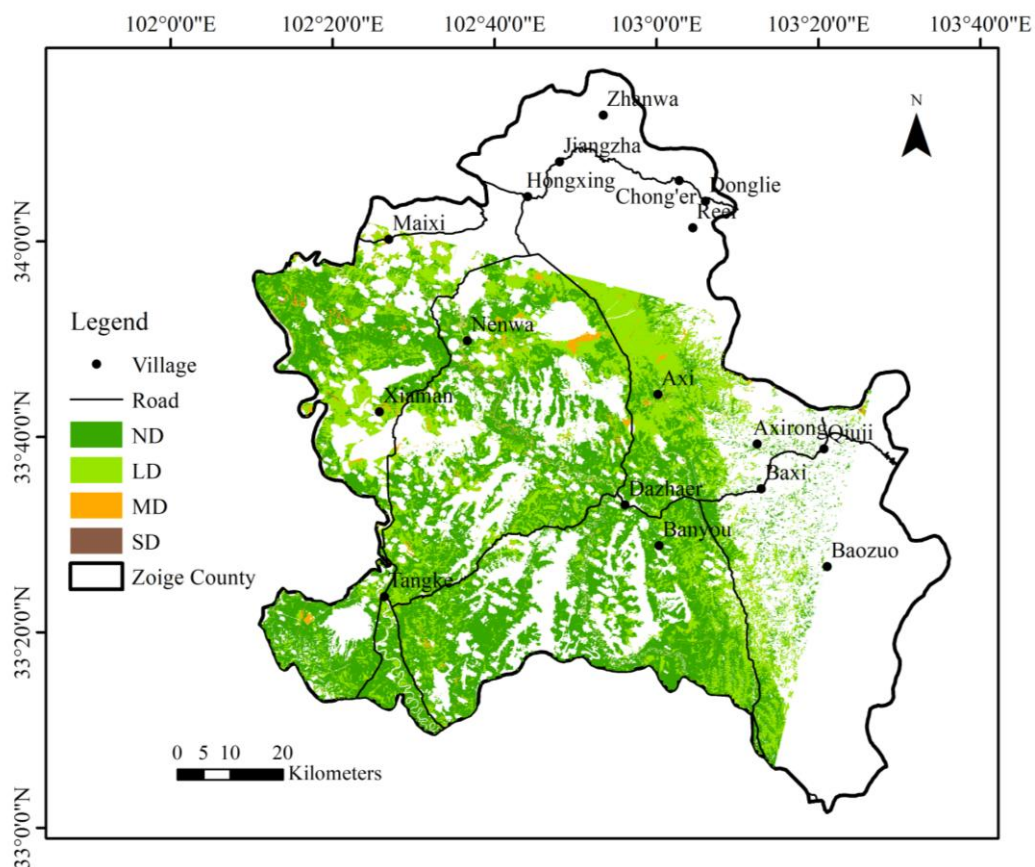
Figure 7 Spatial distribution of alpine grassland desertification index (AGDI) in the part of Zoige. SD: severe desertification, MD: moderate desertification, LD: light desertification, and ND: non-desertification. The blank areas include other land types and masks of clouds and cloud shadows.

1432

Table 5 Confusion matrix of the predicted Alpine Grassland Desertification Index (AGDI) and in situ AGDI.

		In situ AGDI				
	Degree	Severe	Moderate	Light	No	Total
	Severe	11	2	0	0	13
Predicted AGDI	Moderate	0	8	0	0	8
	Light	0	0	6	2	8
	No	0	0	3	7	10
	Total	11	10	9	9	39

Table 6 Accuracy evaluation of the image classification using the confusion matrix.

Desertification degree	User's accuracy	Producer's accuracy	Overall accuracy
Severe	84.62%	100.00%	
Moderate	100.00%	80.00%	82.05%
Light	75.00%	66.67%	
No	70.00%	77.78%	

the confusion is mainly on LD and ND. The main reason is that the remote sensing features of severe desertification land are distinct and easy to discriminate. However, the classification of light desertification/non-desertification land is susceptible to atmospheric conditions and other factors, such as thin clouds and mixed pixel.

Table 7 shows the AGDI statistics. A total of 4 489.79 km² of grasslands in the study area are investigated after being masked. Severe desertification land (AGDI = 1) accounts for 0.26%, mainly distributed in Xiaman, Nenwa, and Maixi in the northwest of Zoige County. Moderate desertification land (AGDI = 2) comprises 1.72%, mostly in the outer edge of severe desertification land. Light desertification land (AGDI = 3) accounts for 36.96% of the total area, and most are concentrated in Axi, which is northeast of Zoige County. Non-desertification grasslands (AGDI = 4) have the largest proportion, which account for 61.06%, and are distributed throughout the county.

4 Discussion

AGDI was constructed by integrating the characteristics of vegetation and soil in alpine grassland desertification. In some studies, the identification of desertification has generally relied on single indicators, such as VF, AGB, or net primary productivity, which do not fully indicate the characterization of grassland desertification (Zhang et al. 2014; Han et al. 2018). In addition,

different from some studies that directly use remote sensing index to monitor desertification, we establish regression models between remote sensing index and ecological indicators (Becerril-Pina et al. 2016; Lamqadem et al. 2018). Four ecological indicators are estimated by these models, which are most relevant to the signs of desertification. These ecological indicators discuss the ecological significance of AGDI and easy to promotes in other regions. Furthermore, geo-detector is used to reselect and weigh the indicators constructing AGDI for the first time. Ideal results were obtained. To revalidate the identification of SD, 32 points are randomly selected in a severe desertification area. The verification accuracy of SD is 100%, which means that this index is accurate for the identification of severe desertification land. Moreover, the AGDI results on both sides of the river are consistent with natural laws. Under the centrifugal force of water flow, the concave bank is eroded, and the eroded sediment is transported to the opposite bank. Figure 8 clearly shows the accumulation process on the inside of the convex bank.

Table 7 Alpine grassland desertification index (AGDI) statistics in the study area. It showed the area of different degree of grassland desertification and the proportion of total statistical area.

AGDI	Desertification degree	Area (km²)	Proportion (%)
1	Severe	11.65	0.26
2	Moderate	77.44	1.72
3	Light	1 659.49	36.96
4	No	2 741.21	61.06

The area of pattern spots measuring less than 1 km² is calculated. The area measures 1,023.76 km², which accounts for 22.72% of the resulting area. Among them, the area of pattern spots with less than 1 km² for SD/MD accounts for over 90%. The desertification of alpine grasslands is characterized by fragmentation in the eastern Qinghai–Tibetan Plateau. The part of the pattern spots is difficult to be recognized by MODIS data or other low-resolution images. From the above analysis, the 30 m or higher resolution images are suitable for alpine grassland desertification monitoring in humid or semi-humid climatic conditions(Wen et al. 2010).However, The higher the spatial resolution of the remote sensing data, the lower the temporal resolution. In the comparative study of

1433
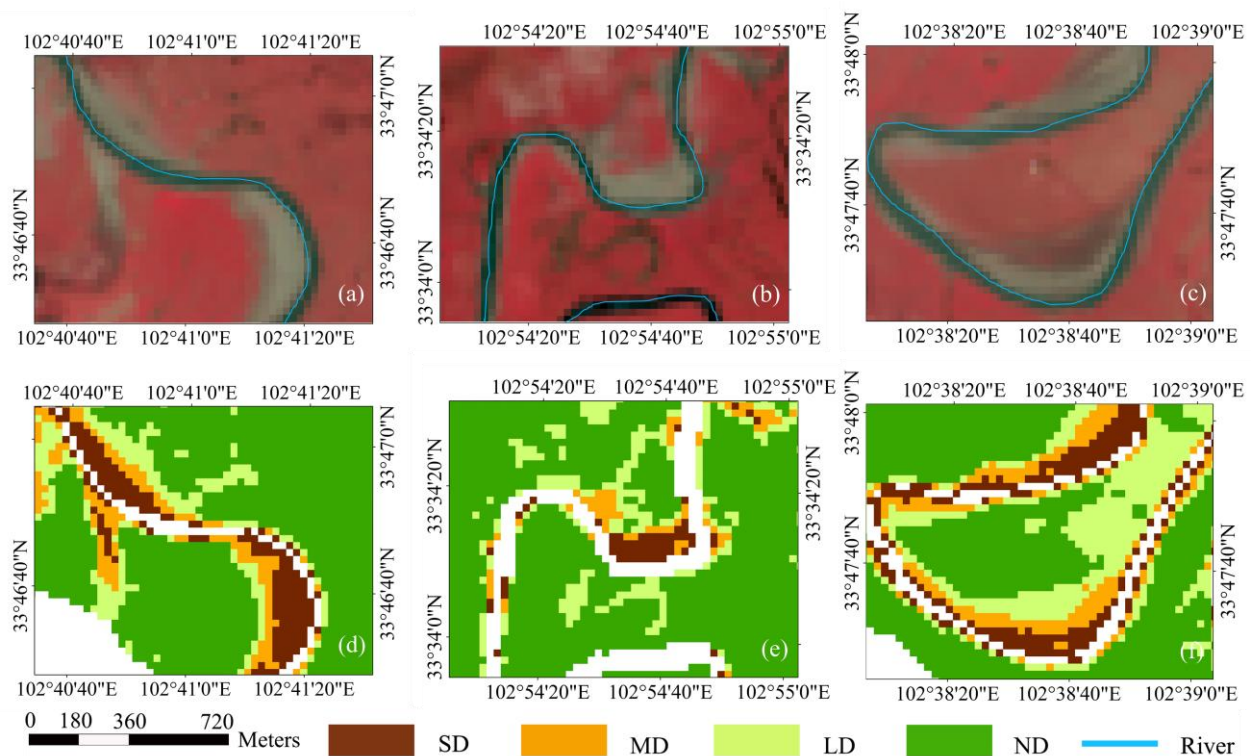
Figure 8 Alpine grassland desertification index (AGDI) results on both sides of the river and corresponding remote sensing images in the study area. (a), (b) and (c) are the RGB (red, green, blue) composite of Landsat bands 5, 4, and 3: the redder the color, the better the vegetation, and the closer the color to gray, the worse the vegetation. (d), (e) and (f) show the results of AGDI derived from (a), (b) and (c) respectively. SD: severe desertification, MD: moderate desertification, LD: light desertification, and ND: non-desertification. The blank areas include other land types and masks of clouds and cloud shadows.

grassland desertification in multiple time series, remote sensing data is susceptible to the effects of cloud contamination and other poor atmospheric conditions. Although the spatial resolution of Modis data is low, MODIS data can provide highly frequent (daily) observations. The influence of clouds and atmosphere can be avoided by Maximum Value Composite method using multiple time series data. Therefore, Modis data have a greater advantage than the data with high spatial resolution when used for the comparative study of time series grassland desertification (Gur and Zalevsky 2011).

In this study, AGDI has a few limitations. (1) The desertification state of a certain moment by one remote sensing image was studied. However, the state of grassland desertification is not stable. Thus, desertification will alleviate/aggravate under the comprehensive effects of climate and human activities. Multiple images for the dynamic monitoring should be used. At this time, adding climate and human factors according to the length

of the study period should be considered. At a short time-intervals, the influence of climate and human factors is approximately the same (the shorter the time-interval is, the more similar), and the effect of climate and human factors can be relatively reduced. (2) The herbaceous swamp is susceptible to the spectral characteristics of the water body. This type of land is classified as SD/MD. Therefore, AGDI is applicable to alpine steppes or alpine meadows, and is not suitable for herbaceous marshes. (3) NDVI and AGB are closely related to plant growth. We need to have prior knowledge of the situation in study area, especially the plant growth period, to select the best time to obtain field data. To distinguish the characteristics of desertification and non-desertification area, we recommend use the images of vegetation growing season to study desertification. In addition, monitoring dynamic changes of desertification should compare the state of same plant period in different years. (4) For remote sensing images, the spectral characteristics are susceptible to sensors,

1434

clouds, and solar elevation angles. This study masked the clouds and the shadow of clouds, which to some extent affect the overall evaluation of the study area. The coverage of thin clouds entails a part of non-desertification land classified light desertification land. Moreover, mixed pixels relatively affect the accuracy of AGDI. Despite some limitations, the novel tool used in this study can provide valuable reference for grassland desertification monitoring.

5 Conclusion

This study proposes an index called Alpine Grassland Desertification Index (AGDI), which is a novel tool to monitor alpine grassland desertification and identify areas at risk of desertification. Vegetation fraction (VF), aboveground biomass (AGB), soil moisture (SM), and land surface temperature (LST) are selected to construct the comprehensive index, which are the most important characteristics of desertification in alpine grasslands. Regression models are used in the estimation of the four indicators, and the suitable remote sensing index are selected by regression analysis. Thereafter, a geo-detector is used to reselect and weight these indicators. LST is excluded because it had the weakest interpretation of AGDI.

AGDI is introduced in Zoige County. The following conclusions are obtained. Geo-detector is used to construct grassland desertification index for the first time. Ideal results are obtained. The overall verification accuracy of classification is 82.5%, and the accuracy of identifying severe desertification reaches 100%. Moreover, fragmentation distribution is the characteristic of alpine grassland desertification in the eastern Qinghai–Tibetan Plateau. Landsat-8 OLI data with a spatial resolution of 30 m are more suitable for desertification monitoring than MODIS data or other low-resolution images in this study. The findings are relevant for evaluating grassland desertification in the eastern Qinghai–Tibetan Plateau. Therefore, we can try to introduce AGDI in other grassland regions in the world. AGDI can be used to monitor the performance of grassland management policy. In addition, considering the development of animal husbandry in alpine grasslands, future efforts are needed to explore how grassland desertification affects animal husbandry economy, and the relationship between grassland desertification and grazing behavior.

Acknowledgements

References

Bai L, Jiang L, Yang DY, et al. (2019) Quantifying the spatial heterogeneity influences of natural and socioeconomic factors and their interactions on air pollution using the geographical detector method: a case study of the Yangtze River economic belt, China. Journal of Cleaner Production 232: 692-704. https://doi.org/10.1016/j.jclepro.2019.05.342

Becerril PR, Diaz DC, Mastachi LCA, et al. (2016) Integration of remote sensing techniques for monitoring desertification in Mexico. Human and Ecological Risk Assessment 22(6): 1323-1340. https://doi.org/10.1080/10807039.2016.1169914

Bestelmeyer BT, Okin GS, Duniway MC, et al. (2015) Desertification, land use, and the transformation of global drylands. Frontiers in Ecology and the Environment 13(1): 28-36. https://doi.org/10.1890/140162

Brinkmann K, Dickhoefer U, Schlecht E, et al. (2011) Quantification of aboveground rangeland productivity and anthropogenic degradation on the Arabian Peninsula using Landsat imagery and field inventory data. Remote Sensing of Environment 115(2): 465-474. https://doi.org/10.1016/j.rse.2010.09.016

Cao XM, Feng YM, Wang JL (2017) Remote sensing monitoring the spatio-temporal changes of aridification in the Mongolian Plateau based on the general Ts-NDVI space, 1981-2012. Journal of Earth System Science 126(4): 58-74. https://doi.org/10.1007/s12040-017-0835-x

Chang S, Wu BF, Yan NN, et al. (2017) Suitability assessment of satellite-derived drought indices for Mongolian grassland. Remote Sensing 9(7):650-673. https://doi.org/10.3390/rs9070650

Chang XF, Zhu XX, Wang SP, et al. (2012) Temperature and moisture effects on soil respiration in alpine grasslands. Soil Science 177(9): 554-560. https://doi.org/10.1097/SS.0b013e31826bdd5d

Chu D. (2018) MODIS remote sensing approaches to monitoring soil moisture in Tibet, China. Remote Sensing Letters 9(12): 1148-1157. https://doi.org/10.1080/2150704x.2018.1516308

Del Valle HF, Elissalde NO, Gagliardini DA, et al. (2014) Status of desertification in the Patagonian region: assessment and mapping from satellite imagery. Arid Soil Research and

Rehabilitation 12: 95-121.
https://doi.org/10.1080/15324989809381502

Demarez V, Duthoit S, Baret F, et al. (2008) Estimation of leaf area and clumping indexes of crops with hemispherical photographs. Agricultural & Forest Meteorology 148(4): 644-655. https://doi.org/10.1016/j.agrformet.2007.11.015

Development Planning Department of Agriculture (2003) 2001-2010 National grassland ecological protection construction planning. Pratacultural Science 20(9):80-84. (In Chinese)

Dong ZB, Hu GY, Yan CZ, et al. (2010) Aeolian desertification and its causes in the Zoige Plateau of China's Qinghai-Tibetan Plateau. Environmental Earth Sciences 59(8): 1731-1740.
https://doi.org/10.1007/s12665-009-0155-9

Du ZQ, Xu XM, Zhang H, et al. (2016) Geographical detector-based identification of the impact of major determinants on aeolian desertification risk. Plos One 11(3):1-18.
https://doi.org/10.1371/journal.pone.0151331

Gur E, Zalevsky Z (2011) Resolution-enhanced remote sensing via multi spectral and spatial data fusion. International Journal of Image and Data Fusion 2(2):149-165.
https://doi.org/10.1080/19479832.2010.551520

Foody GM (2002) Status of land cover classification accuracy assessment. Remote Sensing of Environment 80(1): 185-201.
https://doi.org/10.1016/s0034-4257(01)00295-4

Galindo ICD, Ribeiro MR, Santos MDDV, et al. (2008) Soils and vegetation relations in areas under desertification in Jatauba county, Pernambuco State, Brazil. Revista Brasileira De Ciencia Do Solo 32(3): 1283-1296.
https://doi.org/10.1590/S0100-06832008000300036 (In Portuguese)

Gao QZ, Wan YF, Xu HM, et al. (2010) Alpine grassland degradation index and its response to recent climate variability in Northern Tibet, China. Quaternary International 226(1-2): 143-150.
https://doi.org/10.1016/j.quaint.2009.10.035

Gou XL, Tu WG, Li L, et al. (2016) Research on characteristics of the desertified grassland in the north-west of sichuan province. Acta Agrestia Sinica 24(04): 768-775. (In Chinese)

Han DM, Wang GQ, Xue BL, et al. (2018) Evaluation of semiarid grassland degradation in North China from multiple perspectives. Ecological Engineering 112: 41-50.
https://doi.org/10.1016/j.ecoleng.2017.12.011

He BB, Liao ZM, Quan XW, et al. (2015) A global grassland drought index (GDI) product: algorithm and validation. Remote Sensing 7(10): 12704-12736.
https://doi.org/10.3390/rs71012704

He JN, Xu J, Kang WX, et al. (2016) Evolution Dynamic characteristics of land desertification in Zoige county, China. Scientia Silvae Sinicae 52(1):159-165. (In Chinese)

Hengl T, Heuvelink GBM, Tadic MP, et al. (2012) Spatio-temporal prediction of daily temperatures using time-series of MODIS LST images. Theoretical and Applied Climatology 107(1-2): 265-277.
https://doi.org/10.1007/s00704-011-0464-2

Hu GY, Dong ZB, Lu JF, et al. (2013) Aeolian desertification and its landscape pattern change in the Zoige basin, Qinghai-Tibet Plateau during 1975-2005. Journal of Desert Research 33(1): 16-23.
https://doi.org/10.7522/j.issn.1000-694x.2013.00003

Huang S, Siegert F (2006) Land cover classification optimized to detect areas at risk of desertification in North China based on SPOT VEGETATION imagery. Journal of Arid Environments 67(2): 308-327.
https://doi.org/10.1016/j.jaridenv.2006.02.016

Jin YX, Yang XC, Qiu JJ, et al. (2014) Remote sensing-based biomass estimation and its spatio-temporal variations in temperate grassland, northern China. Remote Sensing 6(2): 1496-1513. https://doi.org/10.3390/rs6021496

Kauth RJ, Thomas GS (1976) The tasselled cap -- a graphic description of the spectral-temporal development of agricultural crops as seen by Landsat. In: Proceedings of the Symposium on Machine Processing of Remotely Sensed Data, Purdue University, West Lafayette, USA. pp. 41-51

Kuang SA, Tian SF, Chen B (2002) Remote sensing monitoring of land desertification in the agriculture and graziery mixed area. Remote Sensing for Land & Resources 02: 10-14. (In Chinese)

Lamqadem AA, Saber H, Pradhan B (2018) Quantitative assessment of desertification in an arid oasis using remote sensing data and spectral index techniques. Remote Sensing 10(12):1862. https://doi.org/10.3390/rs10121862

Li JY, Yang XC, Jin YX, et al. (2013) Monitoring and analysis of grassland desertification dynamics using Landsat images in Ningxia, China. Remote Sensing of Environment 138: 19-26.
https://doi.org/10.1016/j.rse.2013.07.010

Li MM (2003) The method of vegetation fraction estimation by remote sensing. Master thesis, institute of remote sensing applications Chinese academy of sciences, Beijing, China. (In Chinese)

Li XR, Jia XH, Dong GR (2006) Influence of desertification on vegetation pattern variations in the cold semi-arid grasslands of Qinghai-Tibet plateau, North-west China. Journal of Arid Environments 64(3): 505-522.
https://doi.org/10.1016/j.jaridenv.2005.06.011

Li YN, Zhang L, Liao JJ, et al. (2013) Remote sensing monitoring of grassland degradation in the central of the northern Tibet. Remote Sensing Technology and Application 28(06): 1069-1075. (In Chinese)

Li ZY, Liu XH, Ma TX, et al. (2013) Retrieval of the surface evapotranspiration patterns in the alpine grassland-wetland ecosystem applying SEBAL model in the source region of the Yellow River, China. Ecological Modelling 270: 64-75.
https://doi.org/10.1016/j.ecolmodel.2013.09.004

Mansour K, Mutanga O, Adam E, et al. (2016) Multispectral remote sensing for mapping grassland degradation using the key indicators of grass species and edaphic factors. Geocarto International 31(5): 477-491.
https://doi.org/10.1080/10106049.2015.1059898

Ministry of agriculture. (2003) Classification index standard of natural grassland degradation, desertification and salinization. Agriculture Press, Beijing, China. (In Chinese)

Mougin E, Demarez V, Diawara M, et al. (2014) Estimation of LAI, fAPAR and fCover of Sahel rangelands (Gourma. Mali). Agricultural and Forest Meteorology 198:155-167.
https://doi.org/10.1016/j.agrformet.2014.08.006

Qiu (2016) Trouble in Tibet: Rapid changes in Tibetan grasslands are threatening Asia's main water supply and the livelihood of nomads.
https://www.nature.com/news/trouble-in-tibet-1.19139
(Accessed on 2019-08-21)

Qin XJ, Sun J, Liu M, et al. (2016) The impact of climate change and human activity on net primary production in Tibet. Polish Journal of Environmental Studies 25(5): 2113-2120.
https://doi.org/10.15244/pjoes/62986

Reynolds JF, Stafford SDM, Lambin EF, et al. (2007) Global desertification: Building a science for dryland development. Science 316(5826): 847-851.
https://doi.org/10.1126/science.1131634

Rossi M, Niedrist G, Asam S, et al. (2019) A comparison of the signal from diverse optical sensors for monitoring alpine grassland dynamics. Remote Sensing 11(3): 296-318.
https://doi.org/10.3390/rs11030296

Rubio JL, Bochet E (1998) Desertification indicators as diagnosis criteria for desertification risk assessment in Europe. Journal of Arid Environments 39(2): 113-120.
https://doi.org/10.1006/jare.1998.0402

Schlesinger WH, Reynolds JF, Cunningham GL, et al. (1990) Biological feedbacks in global desertification. Science 247(4946): 1043-1048.
https://doi.org/10.1126/science.247.4946.1043

Sepehr A, Zucca C (2012) Ranking desertification indicators using TOPSIS algorithm. Natural Hazards 62(3): 1137-1153.
https://doi.org/10.1007/s11069-012-0139-z

Shui W, Bai JP, Jian XP, et al. (2017) Changes in water

conservation and soil physicochemical properties during the recovery of desertified grassland in Zoigê, China. Acta Ecologica Sinica 37(01): 277-285. https://doi.org/10.5846/stxb201607221492 (In Chinese)

Stuckens J, Coppin PR, Bauer ME (2000) Integrating contextual information with per-pixel classification for improved land cover classification. Remote Sensing of Environment 71(3): 282-296. https://doi.org/10.1016/s0034-4257(99)00083-8

Tsunekawa A, Ito TY, Shinoda M, et al. (2005) Methodology for assessment of desertification based on vegetation degradation using net primary productivity (NPP) as a key indicator. Phyton-Annales Rei Botanicae 45(4): 185-192.

Wang JF (2017) Geodetector. http://www.geodetector.cn/(Accessed on 2019-08-21)

Wang HJ, Fan WJ, Cui YK, et al. (2010) Hyperspectral remote sensing monitoring of grassland degradation. Spectroscopy and Spectral Analysis 30(10): 2734-2738. https://doi.org/10.3964/j.issn.1000-0593(2010)10-2734-05

Wang J, Ling ZW, Wang Y, et al. (2016) Improving spatial representation of soil moisture by integration of microwave observations and the temperature-vegetation-drought index derived from MODIS products. ISPRS Journal of Photogrammetry and Remote Sensing 113: 144-154. https://doi.org/10.1016/j.isprsjprs.2016.01.009

Wang JF, Xu CD (2017) Geodetector: Principle and prospective. Acta Geographica Sinica 72(01): 116-134. (In Chinese)

Wang JF, Zhang TL, Fu BJ (2016) A measure of spatial stratified heterogeneity. Ecological Indicators 67: 250-256. https://doi.org/10.1016/j.ecolind.2016.02.052

Wang JY, Li AN, Bian JH (2016) Simulation of the grazing effects on grassland aboveground net primary production using DNDC model combined with time-series remote sensing data-a case study in Zoige Plateau, China. Remote Sensing 8(3): 168-188. https://doi.org/10.3390/rs8030168

Wang LW, Wei YX, Niu Z (2008) Grassland classification in Naqu prefecture of Tibet. A Journal of the Human Environment 37(4): 322-324. https://doi.org/10.1579/0044-7447(2008)37[322:GCINPO]2.0.CO;2

Wang M, Yang G, Gao YH, et al. (2015) Higher recent peat C accumulation than that during the Holocene on the Zoige Plateau. Quaternary Science Reviews 114: 116-125. https://doi.org/10.1016/j.quascirev.2015.01.025

Wang RB, Zhang NN, Wang QQ (2016) The method research and application of desertification land monitoring. Geomatics&Spatial Information Technology 39(10): 163-166. (In Chinese)

Wen QK, Zhang ZX, Liu S, et al. (2010) Classification of grassland types by MODIS time-series images in Tibet, China. IEEE Journal of Selected Topics in Applied Earth Observations and Remote Sensing 3(3): 404-409. https://doi.org/10.1109/Jstars.2010.2049001

Yu CQ, Zhang XZ, Zhang J, et al. (2016) Grazing exclusion to recover degraded alpine pastures needs scientific assessments across the Northern Tibetan Plateau. Sustainability 8(11):1162-1168. https://doi.org/10.3390/su8111162

Yu KF, Lehmkuhl F, Falk D (2017) Quantifying land degradation in the Zoige Basin, NE Tibetan Plateau using satellite remote sensing data. Journal of Mountain Science 14(1): 77-93. https://doi.org/10.1007/s11629-016-3929-z

Yuan QZ, Wu SH, Dai EF, et al. (2017) Spatio-temporal variation of the wet-dry conditions from 1961 to 2015 in China. Science China-Earth Sciences 60(11): 2041-2050. https://doi.org/10.1007/s11430-017-9097-1

Yue DX, Zeng JJ, Yang C, et al. (2018) Ecological risk assessment of the Gannan Plateau, northeastern Tibetan Plateau. Journal of Mountain Science 15(6): 1254-1267. https://doi.org/10.1007/s11629-017-4466-0

Zanchetta A, Bitelli G, Karnieli A (2016) Monitoring desertification by remote sensing using the Tasselled Cap transform for long-term change detection. Natural Hazards 83(1): 1-15. https://doi.org/10.1007/s11069-016-2342-9

Zhang BH, Zhang L, Xie D, et al. (2016) Application of synthetic NDVI time series blended from Landsat and MODIS data for grassland biomass estimation. Remote Sensing 8(1):1-21. https://doi.org/10.3390/rs8010010

Zhang X, Shang K, Cen Y, et al. (2014) Estimating ecological indicators of karst rocky desertification by linear spectral unmixing method. International Journal of Applied Earth Observation and Geoinformation 31: 86-94. https://doi.org/110.1016/j.jag.2014.03.009

Zhang X, Zhao WW, Liu YX, et al. (2016) The relationships between grasslands and soil moisture on the Loess Plateau of China: A review. Catena 145: 56-67. https://doi.org/10.1016/j.catena.2016.05.022

Zhang XK, Lu XY, Wang XD (2014) The spatial and temporal variation of NDVI and its relationships to climatic factors in Northern Tibet over the period of 2000-2010----Take Shantsa for example. Mountain Research 32(04): 475-480. (In Chinese)

Zhang XL, Zhao Y. (2018) Identification of the driving factors' influences on regional energy-related carbon emissions in China based on geographical detector method. Environmental Science and Pollution Research 25(10): 9626-9635. https://doi.org/10.1007/s11356-018-1237-6

Zhang Y, Zhang CB, Wang ZQ, et al. (2019) Comprehensive research on remote sensing monitoring of grassland degradation: a case study in the three-river source region, China. Sustainability 11(7): 1845-1852. https://doi.org/10.3390/su11071845

Zhang ZC, Hou G, Liu M, et al. (2019) Degradation induces changes in the soil C:N:P stoichiometry of alpine steppe on the Tibetan Plateau. Journal of Mountain Science 16(10): 2348-2360. https://doi.org/10.1007/s11629-018-5346-y

Zhao GH, Dan ZTQ, Wei XD (2012) A review grassland desertification characteristics of Qinghai-Tibet Plateau. Grassland and Turf 32(5): 83-89. (In Chinese)

Zhou W, Yang H, Huang L, et al. (2017) Grassland degradation remote sensing monitoring and driving factors quantitative assessment in China from 1982 to 2010. Ecological Indicators 83: 303-313. https://doi.org/10.1016/j.ecolind.2017.08.019